

# CHARACTERIZATION OF CORROSION RELATED FAILURES

S. R. Singh

Materials Characterization Division

National Metallurgical Laboratory

Jamshedpur - 831 007

## Abstract

This paper deals with the characterization of corrosion related failures of structural steel components in the various environments of petrochemical industries. The case studies, pertaining to the failures due to, stress corrosion cracking in CO<sub>2</sub> environment, catastrophic carburization (metal dusting corrosion) in hydrocarbon environment, and corrosion fatigue in steam environment have been discussed.

The cracking in the linepipe (conforming to IS1239) was due to grain boundary segregation of Mn and Si leading to hardening in the region just outside the outermost area of HAZ, i.e., SCHAZ and in the parent metal. The service cracking as well as tensile test fracture always occurred in parent metal with different degree of intergranular brittle fracture. The factors that directly affect the occurrence of cracks are due to; segregation of Mn & Si outside the HAZ, longitudinal stress as well as residual stress due to weld and corrosive nature of CO<sub>2</sub>-CO-H<sub>2</sub>O system. These three factors satisfies the occurrence of SCC.

A failed reactor tube of 1.25Cr-0.5Mo steel have been investigated. The characterization of corrosion products revealed the presence of wustite, magnetite, Cr<sub>2</sub>C, M<sub>23</sub>C<sub>6</sub>, rounded metal particles and carbon soot. The morphological feature in the subsurface region revealed highly carburized inner tube metal surface. This carburized layer was indicative of non-protective behavior of oxide scale in the operative temperature and environment. In the thicker region of tube wall, thinning in the form of rounded pits whereas in the thinner region of tube, metal loss in the form of uniform thinning was encountered. All these observations indicate that the metal wastage was due to carburizing condition.

The microstructural changes occurred in the steam drum nozzle weld as well as vortex breaker weld, made of a commercial HSLA steel (DIN 15NiCuMoNb5) have been investigated. The welds showed predominantly an acicular ferritic microstructure with dislocation substructure which is beneficial for weld toughness. Various types of intragranular and intergranular precipitates have been observed. However, the ε-Cu precipitates of about 40 nm were observed which is much higher than the 20 nm size often observed in this class of steel, indicating an overaging effect. Large number of spherical aluminosilicate inclusions containing titanium have also been found. The cracks were revealed by SEM which infers the crack propagation direction. The features and service conditions are indicative of corrosion fatigue cracks. The corrosion fatigue cracking resulted from combination of, i) vibration, ii) susceptible microstructure, and iii) corrosive environment.

## §1. INTRODUCTION

Engineering materials are used in environments that are capable of reacting with the material. Amongst all the structural materials, the low alloy steels certainly outnumber all others. Their combination of strength and ductility and the ability to vary both of these properties by straight-forward heat treatment or compositional changes makes them by far the most versatile material available today. To avoid the affect of the material-environment interactions, metallurgist have long been concerned with failure that occur as a result of this interaction. The materials are expected to show maximum performance, provide long life for maximum economy and at the same time ensure safety and reliability of components and systems. For all this, we need to know the causes of failures which pinpoints to the solution of practical problem. As might be expected, the affect of such interactions are quite varied in different environment and a catalogue of such an effect fill pages. What we have chosen to do so is to select three environments which have received particular attention in petrochemical industries and concentrate on them. These are;

- (1) Stress corrosion cracking in CO<sub>2</sub> environment,
- (2) Catastrophic carburization (metal dusting corrosion) in hydrocarbon environment
- (3) Corrosion fatigue in steam environment.

A failure analysis require judicious choice of characterization methodology which consist of following characterization techniques.

- (1) Optical Metallography
- (2) Quantitative Metallography
- (3) Scanning Electron Microscopy
- (4) X-ray Diffractometry
- (5) Transmission Electron Microscopy
- (6) Hardness survey
- (7) Mechanical testing

Depending on the requirement, the characterization methods have been selected. The following case studies describe the various methodology to pin point the cause of failure.

## §2. STRESS CORROSION CRACKING

### 2.1. Material and Background Information:

Over the last two years, a LPG recovery plant, have observed cracking at a number of locations in a portion of 6" diameter inert gas header. The linepipe is made of carbon steel of IS: 1239 specification. The cracking appear to have occurred in circumferential welds or in HAZ. The linepipe has been in service for last seven years and carries inert gas generated in their I. G. plant to various utility points in the unit. They have reported; (1) a marked increased in the CO<sub>2</sub> content of inert gas from 8 vol % to 12 vol % since 1993 onwards, (2) extensive ultrasonic thickness surveys near as well as away from the failure sites revealed uniform thickness, thereby, eliminating any possibility of general / localized corrosion due to the medium, (3) during hydrotest, leakage was observed from one of the seam which was rectified by using seamless pipe and further welding while this appeared to be a solitary case, it does point to some inherent defect in the said pipe segment, either due to faulty material or fabrication.. Three samples of linepipe have been investigated. The samples "A" and "B" have undergone cracking failure and taken from different locations whereas the sample "C" is an uncracked but undergone same service exposure. The details of service conditions and materials specifications are as follows;

Linepipe Material	: Carbon steel conforming IS:1239 (minimum UTS = 320 MPa, % elongation > 20 %, S < 0.05 % and P < 0.05 %).
Pressure	: 7 kg/cm <sup>2</sup> .
Temperature	: 40 °C.
Gas composition	: Nitrogen 88 vol%. Carbon dioxide 12 vol%. Oxygen 0.5 vol%. Carbon monoxide < 0.5 vol%.

The heat affected zone (HAZ) of the single cycle weld can be classified, microstructurally, into four regions depending on the peak temperature experienced. These are grain coarsened HAZ (GHAZ) experiencing temperature above 1100 °C, grain refined HAZ (GRHAZ) facing temperature between 1100 °C to Ac<sub>3</sub>, intercritical HAZ (ICHAZ) between Ac<sub>3</sub> to Ac<sub>1</sub> and subcritical HAZ (SCHAZ) formed at temperature lower than Ac<sub>1</sub>. A schematic illustration of the weld-HAZ microstructural regions of a single pass weld is shown in Fig. 1.

Stress corrosion cracking (SCC) of carbon and low alloy steel is a significant problem for a variety of industries, such as those dealing with power generation, oil and gas, refining and pipeline transmission. SCC is particularly insidious in that catastrophic failures can occur even at low applied stress level (sometimes only residual in nature) and often has no warning. Environment causing SCC can be so mild that no evidence of corrosion can be detected except SCC itself. For SCC to occur in any material, the following three conditions must be satisfied, i.e., (1) sufficient level of tensile stress, (2) a corrosive medium, and (3) susceptible microstructure.

The dry carbon dioxide is noncorrosive to metals and alloys. However in the presence of water, CO<sub>2</sub> forms weak carbonic acid which is corrosive. Most oil and gas production has associated water production, either formation or condensation. CO<sub>2</sub> corrosion is normally of the weight loss type, but CO<sub>2</sub> can, in presence of carbon monoxide (CO) and water, result in

stress corrosion cracking (SCC) of susceptible metals. Mixture of CO<sub>2</sub>, CO and water can cause SCC of plain steels and low alloy steels<sup>(4,5)</sup>. The origin of failure usually being associated with localized corrosion on steels with high Mn-contents.

### **§2.2. Characteristics of CO-CO<sub>2</sub> Stress Corrosion Cracking:**

Based on the experimental program supported by Pipeline Research Committee of American Gas Association, the following characteristics are pertinent to CO-CO<sub>2</sub> stress corrosion cracking of gas transmission pipelines<sup>(6)</sup>.

- (1) CO, CO<sub>2</sub> and H<sub>2</sub>O must be present for SCC.
- (2) CO<sub>2</sub> & CO partial pressures as low as 1 psi can promote CO-CO<sub>2</sub> SCC of pipeline steel.
- (3) Oxygen greatly increases the severity of SCC.
- (4) The severity of SCC increases with increasing CO, CO<sub>2</sub>, decreasing CO, anodic polarization and increasing O<sub>2</sub>.
- (5) Steels with Cr-content greater than 9% have not been shown to be susceptible to CO-CO<sub>2</sub> SCC.

### **§2.3. General Characteristics of SCC Features:**

The following criterion provide a general characterization of SCC features.

- (1) SCC represents a brittle rupture. Brittle fracture and an absence of plastic deformation should generally be present.
- (2) Stresses required for SCC are usually small (below the macroscopic yield stress) and are static and tensile in nature. Applied stresses often add to a residual stress condition.
- (3) SCC cracks initiate on the surface, and numerous initiation sites are possible (in contrast with mechanical failures, which usually have a single preferred site).
- (4) As is characteristic of brittle failures, the general crack path is usually aligned normal to the tensile axis.
- (5) There usually is minimal evidence of corrosion damage. However, surface staining on exposed surfaces may be present.
- (6) SCC is a progressive type of fracture, i.e., cracks grow gradually over a period of time.

### **§2.4. Experimental:**

**§2.4.1. Visual examination & dimensional measurements:** The 6" dia header linepipes were having circumferential weld. The linepipes A & B showed cracks running parallel to weld while linepipe C was a sound tube. All the external surfaces of linepipes were protected by yellow paint. Figure 2 showed a photograph of cracked linepipe where the crack is marked by arrows. The extent of the cracks were about 3" - 4 ". The internal surface of all the tubes exposed to the carrier gases showed adherent brown deposit. The measured dia of the linepipes were 16.5 cm. The carrier gas internal pressure of 10 kg/cm<sup>2</sup> (0.98 MPa) would give rise to hoop stress (tangential stress),  $\sigma_{hoop} = 16.2$  MPa and longitudinal stress,  $\sigma_{longitudinal} = 8.1$  MPa. As the cracks were along the circumference, therefore, the longitudinal stress would be operative on cracks.

**§2.4.2. Chemical analysis:** The composition conforms to IS: 1239 which specify that the phosphorous and sulfur should be less than 0.05%. As shown in the table 1, the weld metal has higher concentration of Mn and Si as compared to the parent metal. The parent metal composition of linepipe B differs from that of A and C in respect of Cr and Si concentration. Therefore the linepipes A and C might belong to same group which certainly differs from the group comprising of linepipe B.

**§2.4.3. Optical metallography and SEM studies:** The samples A/B and C were examined for location of cracks and its corresponding microstructural characteristics. The microstructures of weld, Different areas of HAZ [consisting of coarse grained HAZ (CGHAZ), grain refined HAZ (GRHAZ), intercritical HAZ (ICHAZ) and subcritical HAZ (SCHAZ)] and nearby base metal were characterized. No defects were found in the weld and HAZ. The cracks

were about 2-3 mm away from the SCHAZ and in base metal. The base metal near crack contains grain boundary phases termed 'dark phase' (Fig. 3) because of its atomic number contrast in back scattered electron images. The composition of dark phase and nearby ferrite grains were determined by EDAX. This showed significant segregation of Si and Mn in the dark phase (Table 2). The microhardness of dark phase was much higher than the nearby ferrite grains (Table 3). All these observation showed hardening of grain boundary phase was due to segregation of Mn and Si. The dark phase was only observed in cracked samples. The absence dark phase in virgin sample indicates that its formation occurred during service exposure.

**Table 1: Chemical composition (wt%) of weld and parent metal of linepipe.**

Pipe	Area	C	Mn	Si	P	S	Cr	Cu	Ni	Fe
A	Parent	0.09	0.51	0.03	0.03	0.020	n.f.	0.0070	0.004	balance
A	Weld	0.13	1.22	0.45	0.04	0.018	n.f.	0.016	0.01	balance
B	Parent	0.11	0.54	0.12	0.007	0.020	0.009	0.0085	0.005	balance
B	Weld	0.11	1.24	0.46	0.016	0.018	0.0085	0.0093	0.006	balance
C	Parent	0.11	0.53	0.02	0.02	0.021	n.f.	0.007	0.005	balance
C	Weld	0.13	1.23	0.59	0.04	0.014	n.f.	0.01	0.006	balance

n.f. = not found

**§2.4.4. Compositional analysis by EDAX:** The samples from pipelines A, B & C were analyzed for the partitioning of alloying elements among the various microstructural features by energy dispersive analysis of X-rays (EDAX). The data were collated in table 2. It is evident that the grain boundary dark phase present in the neighborhood of cracks were richer in Si and Mn as compared nearby ferrite grains. The Si enrichment was 3-4 times and Mn enrichment was about 2-3 times of the ferrite grain interior.

**Table 2: EDAX composition for partitioning of elements.**

S.No	Area	Si wt%	Mn wt%	Fe wt%	S wt%	Remarks
1	Weld pool	0.30	1.03	98.67	*	Area analysis
2	HAZ	0.19	0.95	98.86	*	Area analysis
3	Near crack	0.07	0.75	99.17	*	Area analysis
4	Dark phase (pipe-B)	<b>0.44</b>	<b>1.13</b>	98.43	*	Point analysis
5	Dark phase (pipe-A)	<b>0.36</b>	<b>1.40</b>	98.24	*	Point analysis
6	Ferrite grain near crack (pipe-B)	<b>0.10</b>	<b>0.52</b>	99.38	*	Point analysis
7	Ferrite grain near crack (pipe-A)	<b>0.12</b>	<b>0.56</b>	99.33	*	Point analysis
8	Elongated silicate inclusions	15.32	36.64	46.69	1.35	Point analysis
9	Inclusions in fractograph	*		*		Point analysis MnS inclusions

\* below minimum detectable limit.

**§2.4.5. Microhardness measurements:** Vickers microhardness measurements were made on a metallographically polished samples from failed pipeline A and B, at a load of 100 g. The measurements were collated in table 3. A general hardness survey were also made on large number of samples from failed pipelines A, B as well as virgin pipeline C, with Vickers

diamond pyramid. The data were presented in table 4. In failed sample the hardness of weld pool increases while that in HAZ decreases with respect to the virgin sample. The base metal hardness of pipeline A was higher than that of B and C.

**Table 3: Microhardness data.**

S. No.	Phase	Microhardness (sample A)	Microhardness (sample B)
1	Grain boundary dark phase	246.06 HV	274.27 HV
2	Adjacent ferrite grain	144.66 HV	158.51 HV

**Table 4: Variation of Vicker's hardness at 30 Kg load.**

S. No.	Sample Area	Hardness (sample A)	Hardness (sample B)	Hardness (sample C)
1	Weld pool	189 HV	189 HV	175 HV
2	HAZ	128 HV	127 HV	157 HV
3	Parent metal	127 HV	116 HV	117 HV

**§2.4.6. Tensile tests:** The room temperature tensile tests were conducted on samples from linepipes A, B & C and the data were summarized in table 5. The fracture always occurred in the base metal and was about few mm from SCHAZ. The fracture surface of tensile tested sample showed almost dimpled ductile fracture while small area adjacent to only one of surface in the gage length showed intergranular brittle fracture. This surface was found to be a part of inner tube wall. The dimples were associated with MnS inclusions. The fractographic observations were summarized in table 6. The UTS of all the linepipes tested were higher than that of IS: 1239 specification which demands the UTS of at least 320 MPa. Moreover, the strength of cracked linepipes A and B did not vary significantly while the uncracked linepipe C showed comparatively lower strength values. The % elongation of all the linepipes were found to be lower than that of IS: 1239 which was specified at 20 % minimum. The lowest value of elongation with largest standard deviation in linepipe C was indicative of presence of flaws/defects which might be stress corrosion cracks introduced during service. The lowering both UTS and % elongation of linepipe C as compared with linepipes A and B were also indicative of undetectable defects during various NDT tests performed at the site. Therefore, inspite of acceptable level of UTS in all the linepipes, the lowering of % elongation with various degree of standard deviations indicates the presence of defects of various size in the tensile specimens.

**Table 5: Room temperature tensile test results of linepipe A, B and C.**

Linepipe-Test No.	Yield strength (MPa)	UTS (MPa)	% Elongation
A-1	300	377	18
A-2	280	383	24
A-3	290	403	24
<b>A (Mean ± s.d.)</b>	<b>290.0 ± 8.2</b>	<b>387.6 ± 11.1</b>	<b>18.5 ± 1.1</b>
B-1	295	390	13.6
B-2	275	378	14.1
B-3	280	381	15.1
<b>B (Mean ± s.d.)</b>	<b>283.3 ± 8.5</b>	<b>383.0 ± 5.1</b>	<b>14.3 ± 0.6</b>
C-1	255	346	8.3
C-2	275	372	14.8
C-3	255	351	18.7
<b>C (Mean ± s.d.)</b>	<b>261.6 ± 9.4</b>	<b>356.3 ± 11.3</b>	<b>13.9 ± 4.3</b>

**§2.4.7. SEM Fractography:** Service cracked samples from linepipes A and B were examined for the fracture mode evaluation. The cracked surface showed brown deposits which hid the underlying fracture surface. The samples were treated with a specially developed solution which selectively dissolved the metal oxides leaving the lustrous metallic fracture surface unaltered. The resultant fractograph showed 100% intergranular (IG) fracture surface indicating brittle fracture mode due to grain boundary decohesion (Fig. 4). The branched cracking was manifested by the grain boundary cracks. The fracture surface of tensile tested sample showed IG fracture of varying degree in small region near the one edge and along the width of the gage length while rest of the area (major portion) showed dimple rupture (Fig. 5a,b). However out of nine samples tested, only three showed complete dimple rupture. The dimples were associated with MnS inclusions. The inner and outer surfaces as well as the thickness of linepipe were represented by width and thickness of tensile samples respectively. The IG fracture was initiated at one of the surface. Based on optical metallographic observations it was concluded that the IG fracture was originated from the inner surface of tube. The coverage of IG fracture surface in tensile tested samples varies in samples from the same linepipe. This was manifested by the varying degree of scatter in % elongation. A summary of fractographic observations is collated in table 6.

**Table 6: Summary of SEM fractographic observations on fracture surfaces of service failed and tensile tested samples of linepipe A, B and C.**

Linepipe-Test No.	Observations
A (service-failed)	100% intergranular (IG) fracture.
B (service-failed)	,,
A-1 (tensile-test)	Intergranular fracture at a small corner of width of gage length while rest of the area showed dimple rupture.
A-2 (tensile-test)	100% dimple rupture.
A-3 (tensile-test)	IG fracture at a corner (visible by naked eye as dark region) of width of gage length while rest of the area showed dimple rupture.
B-1 (tensile-test)	IG fracture near edge of the gage length while rest of the area showed dimple rupture.
B-2 (tensile-test)	IG fracture at very small region of middle of the gage length while rest of the area showed dimple rupture with cracking.
B-3 (tensile-test)	100% dimple rupture with cracking.
C-1 (tensile-test)	IG fracture near the edge (visible by naked eye as three elliptical dark region) while rest of the area showed dimple rupture.
C-2 (tensile-test)	100% dimple rupture.
C-3 (tensile-test)	IG fracture at very small corner area while rest of the area showed dimple rupture.

### **§2.5. Discussions:**

The material chemistry and microstructural effects on intergranular stress corrosion cracking (IGSCC) can generally be divided into two categories: (1) grain boundary precipitation and, (2) grain boundary segregation. Grain boundary precipitation effects include carbide precipitation in austenitic stainless steel and nickel base alloys, which causes a depletion of chromium adjacent to the grain boundary and intermetallic precipitation in aluminum alloys, which are anodically active. Grain boundary segregation of impurities such as P, S, C, and Si can produce a grain boundary that is upto 50% impurity within a region few nm thick . These impurities can alter the corrosion and mechanical properties of the grain boundary and can therefore cause cracking by anodic dissolution and perhaps mechanical fracture. Therefore, an intergranular stress corrosion crack can propagate along grain boundary that has composition vastly different from that of the bulk alloy. It is generally accepted rule of resistance to carbon and low alloy steels to SCC is to maintain hardness below 22 HRC (= 248 HV). This was maintained throughout the weld, HAZ and parent metal. However the grain

boundary segregation outside the HAZ region resulted in the hardness increase in the localized area creating conditions susceptible to SCC.

### **§2.6. Conclusions:**

The cracking in the linepipe was due to grain boundary segregation of Mn & Si leading to hardening in the region just outside the outermost area of HAZ, i.e., SCHAZ and in the base metal. The rigidity of restrained joints can cause cracking. The factors which directly affect the occurrence of cracks are due to compositional factors rather than procedural factors related with welding operations. The surest method for control of CO<sub>2</sub>-CO-H<sub>2</sub>O SCC is to prevent condensation by controlling gas composition and keeping the service temperature above the dew point.

## **§3. CATASTROPHIC CARBURIZATION (METAL DUSTING)**

### **§3.1. Material and Background Information:**

A failure of reactor tube made of 1.25Cr-0.5Mo steel had occurred after a service of 67,000 hours. The failed 6" dia Pacol reactor tube conforms to Sch. 40 ASTM A335-P11. In the process the paraffin hydrocarbon mixed with recycled hydrogen goes into Pacol reactor in vapor state. The material and service conditions are summarized below;

Alloy composition:	Conforms to Sch. 40 ASTM-A335-P11 (1.25Cr-0.5Mo steel).
Dimension of tube:	168.3 mm OD x 7.2 mm thick.
Temp. of outer surface:	Heater inside temperature is 1200 °C near burner combustion zone and is gradually comes down to about 700 °C in convection zone of the heater.
Atmosphere around tube:	Hot air due to combustion of fuel at normal atm. pressure.
Fluid inside tube:	Paraffin.
Inlet temp. of paraffin:	380 °C
Outlet temp. of Paraffin:	490°C
Pressure inside tube:	2 Kg/cm <sup>2</sup> .

In petrochemical industries, the life controlling conditions are usually governed by;

- (1) Creep rupture damage.
- (2) Thermal shock.

In addition to creep damage, and the effects of the higher temperatures, the life of coil alloys is also dependent on; (1) Carburization, (2) Oxidation, (3) Thermal shock due to cycling.

Carburization is observed in several industrial processes under carbonaceous atmosphere at high temperature. Carbon is transferred from gas atmosphere to the alloy matrix, and internal carbides are formed. Usually, the alloys are protected against carburization by an oxide layer barrier against carbon ingress. The oxide scale breakdown occur by chemical reaction or mechanical failure. Metal dusting is a catastrophic carburization <sup>(7,8)</sup> which is a particularly aggressive form of high temperature corrosion of Fe, Co and Ni based alloys by sulfur free mixtures of hydrocarbon in which metal disintegrates into dust of metals, metal carbides, oxides and carbon. This phenomenon is dependent on large number of factors, i.e., gaseous phase composition, temperature, pressure, alloy type and component shape. This is a form of rapid metal wastage in carbonaceous gas streams e.g., CO/CO<sub>2</sub>, hydrocarbons etc., generally in the temperature range 400 - 800 °C. The wastage is often in the form of rounded pits, but in some cases metal loss in the form of uniform thinning is encountered, particularly where gas velocities are high. The surface from which metal is lost are generally carburized, in fact, in almost every case where wastage is of the pitting type, though often it is more difficult to detect carburization if the wastage is of uniform variety in high velocity gas stream. The initiation of carburization process is manifested by presence of sooty deposit containing carbon, metal particles, metal carbide and oxides. This is known to occur with materials based on the Fe, Cr and Ni which are known to have pronounced catalytic effects on the breakdown of CO and hydrocarbon in certain high temperature ranges.

### **§3.2. Characteristics of Catastrophic Carburization:**

The common characteristics of catastrophic carburization (metal dusting corrosion) are summarized below;

Environment:	A gas phase, potentially carburizing and reducing, with or without oxygen-containing components.
Temperature:	400 - 800 °C.
Form of deterioration:	Localized or general pitting, or more general overall wastage. The surface from which metal is lost are carburized.
Corrosion products:	Dust or powder component of carbon mixed with metal, metal carbides, and metal oxides.

### **§3.3. Experimental:**

**§3.3.1. Visual examination:** The transverse section of failed tube is shown in Fig. 6. Wall thickness of tube was non-uniform having maximum thickness of 6.8 mm (region "A") and minimum thickness of 3.6 mm (region "B"). These two regions are diametrically opposite and outer diameter across it was 170 mm while outer diameter perpendicular ("CD") to it was 168 mm. Inner tube surface has dull black appearance with sooty deposits. Therefore the tube had undergone 1% expansion along "AB", where wall thinning was maximum while there was no appreciable deformation along "CD". These observations indicate that the failure would have taken place due to non-uniform wall thinning.

**§3.3.2. Optical metallography:** Microstructures of base metal as well as matrix/scale interface, in transverse section of tube, were analysed. The matrix have usual microstructure consisting of ferrite and tempered bainite. The scale at outer surface was thicker, compact and undamaged with no significant changes in subsurface matrix microstructure, while scale at inner tube surface showed thinner/broken scale with altered subsurface microstructure. These observations indicate that there was breakdown of protective scale which lead to the alteration of subsurface matrix microstructure at the inner wall of tube.

**§3.3.3. Scanning electron microscopy & composition analysis by EDAX:** The inner tube surface/matrix microstructure from transverse section of region "A" is shown in Fig. 7a, which showed the duplex nature of oxide scale consisting of thin inner wustite layer and thick outer magnetite/spinel layer. Ingress of carbon to subsurface region lead to general carburization manifested by intergranular as well as intragranular carbide precipitation/coarsening and initiation of pitting (Fig. 7b). The longitudinal section of inner surface showed (Fig. 8) spherical particles dispersed on irregular shaped particle/soot. SEM of transverse section from region "B" showed unaltered matrix microstructure (Fig. 9a) while subsurface region of inner tube wall showed (Fig. 9b) coarsening of grain boundary precipitates as well as increase in their number density. Also the pitting in region "B" was absent. This indicates that the uniform metal wastage by catastrophic carburization was operative in the region "B".

EDAX analysis of various microstructural constituents have been performed to asses the elemental partitioning. A comparison of composition of base metal with carburized zone showed some enrichment of Mo, Cr and decrease of Si content in carburized zone. The inner and outer oxide scales were enriched with Mo and Si, while Cr content decreased in both scales. The spherical metal particles were also enriched with Mo but Cr content was decreased with respect to base metal.

**§3.3.4. X-ray diffraction analysis:** The analysis of diffractograms, recorded with  $\text{CoK}\alpha$  radiation, from samples of region "A" revealed the presence of ferrite, wustite, magnetite,  $\text{Cr}_2\text{C}$ ,  $\text{M}_{23}\text{C}_6$  and carbon soot. The ferrite peaks originated from base metal as well as spherical metal particles which were formed due to carburization of base metal. Wustite is stable above 570°C and Cr, Mo raises its stability to 600°C. Therefore the presence of wustite in the scale indicates that the region of tube had experienced temperature in excess of 600°C. The absence of hematite, which grow in presence of water vapor and thermodynamically unstable to high reducing gas atmosphere, was consistent with the environment in the tube.

The XRD analysis of samples from region "B" showed the presence of ferrite, magnetite,  $\text{Cr}_2\text{C}$ ,  $\text{M}_{23}\text{C}_6$  while wustite peaks were absent and carbon soot was negligibly small.

### **§3.4. Discussions:**

In catastrophic carburization, i.e., metal dusting, the reaction products are; carbon, carbides and oxides, interspersed with metal particles (poor in Cr). These corrosion products are loosely adherent and can be easily eroded, which lead to, pitting or uniform thinning. The carburization involve following kinetic steps; (1) transport in gas atmosphere by gas flow/diffusion, (2) carbon transfer to the metal phase by phase boundary reaction which are reaction of the gas molecules on the surface, leading to carbon atoms, (3) inward diffusion of dissolved carbon in the metal, (4) reaction of carbon with carbide forming elements in the alloy interior, and diffusion of carbide forming elements to precipitates.

Therefore, carburization resistance can be developed either, (1) by addition of enough silicon (1.5 - 3%) to form more or less continuous sublayer of  $\text{SiO}_2$  beneath the oxide layer which is thermodynamically more stable than oxide and is not attacked by carbon, or, (2) by presence of sulfur which slows down the carbon transfer to the metal surface.

### **§3.5. Conclusions:**

Based on the structural, microstructural and compositional studies conducted on the inside tube wall, the following conclusions can be inferred.

(1) Carburization was manifested by the presence of carbides  $\text{Cr}_2\text{C}$  and  $\text{M}_{23}\text{C}_6$  at the surface and subsurface regions. (2) Phase identified in the region "A" are; ferrite, magnetite, wustite  $\text{Cr}_2\text{C}$ ,  $\text{M}_{23}\text{C}_6$  and carbon soot while in region "B", wustite and carbon soot are absent. (3) Catastrophic carburization in region "B" was of uniform metal wastage type whereas in region "A", it was of pitting type.

Addition of  $\text{H}_2\text{S}/\text{CS}_2$  gas stream acts as catalytic poison for decomposition of hydrocarbon, thereby decreasing the carbon activity and block the ingress of carbon to metallic surface which inhibit carburization process. The material replacement with 5Cr-1Mo/9Cr-1Mo can also results in reduced carburization.

## **§4. CORROSION FATIGUE**

### **§4.1. Material and Background Information:**

At a petrochemical industry, twelve naphtha cracking furnaces and three recycle furnaces were commissioned in March 1997. The leakage in the steam drum was detected in February 1998. During the service period of one year, the drums have experienced seven start up/shut down cycles. The leakages occurred from the through thickness cracks in the welded joints. Large number of radial cracks in the steam drum down comer nozzle welds originated from the inside surface of the steam drum. These cracks were aligned to the longitudinal direction of the steam drum. From their orientation it was clear that all the cracks had developed under the influence of hoop stress and were associated with locally increased stress level. The details of service conditions and materials specifications are as follows;

Steam drum shell & nozzle Material : HSLA steel conforming to DIN designation  
15 NiCuMoNb 5  
Operating temperature : 300 °C  
Operating pressure : 110 atm.  
Steam drum size : 3 m X 1.6 mØ with a wall thickness of 45 mm.

The HSLA steel with good combination of strength, toughness and weldability is usually alloyed with nickel chromium, manganese, molybdenum, niobium and copper. Most of the elements provide hardenability for the transformation of austenite to fine ferritic microstructure in heavy sections. In addition, the strength is enhanced by the precipitation of copper and niobium carbide. This class of steel can be processed to have excellent properties however, problem may still be encountered during welding, in the heat affected zone (HAZ) as well as in the weld metal. The matrix phases in the HAZ transform to austenite and precipitate will coarsen or dissolve during heating cycle; then the matrix will transform to martensite, ferrite, and/or bainite with new precipitate distribution upon cooling<sup>(9-11)</sup>. These changes may

degrade the mechanical properties (e.g., strength, hardness and toughness) of the welded structure. Although there have been a number of studies of HSLA steels within the last ten years, many of these studies have dealt only with mechanical properties supplemented by optical microscopy and/or SEM to correlate the microstructure with the properties. TEM studies usually focused on the effects of alloying elements and/or isothermal aging treatments on the microstructure (10,12) or on the development of continuous cooling transformation (CCT) curves (9,13). However there is still no clear understanding of the detailed microstructures which give rise to the property variation across the weld-HAZ as a function of positioned weld condition, e.g., heat input and preheat.

With these limitations in mind, the present investigation was thus undertaken to study systematically, the detailed microstructural changes which occurred in the weld-HAZ of this class of HSLA steel.

Several failure mechanism have been proposed for the deaerator and steam drum cracking process, including corrosion fatigue cracking, stress corrosion cracking (SCC), strain aging, weld defects, and hydrogen embrittlement. Most reported case studies have substantiated the corrosion fatigue mechanism. Corrosion fatigue refers to the propagation of wedge shaped crack through a metal resulting from cyclic tensile stresses in a corrosive environment. Corrosion fatigue damage frequently occurs in boilers that are in peaking service, operated discontinuously, or operated cyclically. Susceptibility to corrosion fatigue may be enhanced if rapid start ups or shut downs are practiced. Decreasing these rates has alleviated some corrosion fatigue problems in boilers (14). There is one general rule that the greater the uniform corrosion rate the shorter the resultant fatigue life. Therefore metal resistance to corrosion fatigue is associated with its inherent corrosion resistance rather than high mechanical strength. For corrosion fatigue to occur in any material, the following three conditions must be satisfied, i.e., (1) sufficient level of cyclic tensile stress, (2) a corrosive medium, and (3) susceptible microstructure.

#### **§4.2. Characteristic Features of Corrosion Fatigue:**

The corrosion fatigue cracks have following characteristics.

- (1) Wedge-shaped cracks (funnel-mouthed) initiated at pit base and filled with corrosion product.
- (2) Blunted tip.
- (3) Transgranular fracture.
- (4) Limited or no crack-branching.

The crack growth is not one of electrochemical dissolution of metal atoms at the base of the crack. Instead it involves a process of plastic deformation accelerated by corrosion process. This effect is not specific to chloride ions but occurs with any corrosive environment.

#### **§4.3. Experimental:**

**§4.3.1. Transmission electron microscopy:** An extensive thin foil transmission electron microscopy (TEM) examination of all the three weld-HAZ (two vortex breaker weld and a nozzle weld) and parent metal have been carried out. The objective of TEM study was on finding out the microstructural constituents which might have caused the cracking in the welds.

The general microstructure parent metal (PM) consisted of ferrite - bainite with intragranular precipitates of  $\epsilon$ -Cu and cuboid carbonitrides as well as intergranular  $M_3C$  and  $M_7C_3$ . Figure 10 showed a low magnification bright field (BF) micrograph.

The microstructure of vortex breaker weld-1 showed (Fig. 11) mainly acicular ferrite with dislocation substructure within the ferrite plate and above mentioned precipitates. Figure 12 showed higher magnification view of a blocky ferrite grain revealing distribution  $\epsilon$ -Cu precipitates. The average size of these precipitates is about 40 nm and it showed no sign strain contrast around the precipitates. The electron diffraction analysis in conjunction with morphological observations indicates that the precipitates on packet boundaries are cementite.

The general microstructure of vortex breaker weld-2 was found to be similar to that of vortex breaker weld-1. For the sake of clarity, the microstructure corresponding to SCHAZ, ICHAZ and GRHAZ have been analysed. SCHAZ showed typical ferritic microstructure while in the ICHAZ microstructure, ferrite was surrounded by large number of intergranular

carbide precipitates. The GRHAZ microstructures showed inter- and intra-granular carbide precipitation akin to tempered microstructure. The weld metal showed typical acicular ferritic microstructure with dislocation substructure.

The nozzle weld-3 also showed microstructure similar to vortex breaker weld-1 & 2. However, it showed distribution of spherical aluminosilicate inclusions.

**§4.3.2. Scanning electron microscopy:** A low magnification SEM micrograph along with a schematic diagram of cracks in the sample 4BE is shown in Fig. 13. This sample covers the entire region of vortex breaker weld pool and nozzle weld pool with intervening HAZ. The crack initiated (marked by arrow) in vortex breaker weld pool and propagated toward ends A & B. The crack propagating towards the end B followed the two paths; the shorter length crack ended in the weld pool itself while the other longer crack propagated in the neighboring HAZ. A higher magnification montage of photographs is shown in Fig. 14. A localized parallel crack, marked "PC", parallel to main crack is indicated. The features associated with these cracks were indicative of corrosion fatigue crack.

#### **§4.4. Discussions:**

The above results show that the austenite in the HSLA steel transforms to largely ferritic microstructure with variable morphologies and substructures in different regions (different cooling rates) of the weld. Acicular ferrite is defined as a highly substructured, non-equiaxed ferrite that forms on continuous cooling by a mixed diffusion and shear mode of transformation. The level of dislocation density in the acicular ferrite is somewhat lower than that for martensite. The acicular ferrites were arranged in packets with cementite particles at the packet boundaries. Since grain boundary cementite is known to be an embrittler, these cementite precipitates may provide potential fracture paths. Higher carbon HSLA steel which is often associated with thicker plate gages would be most susceptible to this problem. The blocky ferrite usually contains a high density of  $\epsilon$ -Cu precipitates of about 40 nm which is much higher than the 20 nm size often observed in this class of steel. The larger size of  $\epsilon$ -Cu precipitates may be due to overaging effect.

In general terms, the tensile properties of weld metals (with acicular ferrite) are of lesser importance than impact toughness except that a restriction on hardness in welds for pipe intended for sour gas/oil service, usually to a maximum value of 248 VHN, may place some practical limit on UTS. Consequently, there has been relatively much more attention to improving toughness and little need to consider, in detail, strengthening mechanisms in this type of microstructure. There is a critical range in weld metal oxygen content for optimum toughness, as a consequence of this effect the interlocking of acicular ferrite will determine the overall toughness of the weld.

The branching of crack or parallel cracking associated with main cracks are indicative of stress corrosion cracking and corrosion fatigue respectively. The corrosion fatigue cracking results from combination of, i) vibration, ii) susceptible microstructure, and iii) corrosive environment. Such fine parallel cracking usually results from alternating stresses, possibly caused by pressure fluctuations or the effect of water hammer, as well as simple vibration. Repeated expansion and contraction as a result of considerable temperature fluctuations may show similar effects. Corrosion fatigue cracks which result from this cause, are often initiated at small corrosion spots and develop in a transcrystalline manner in contrast to the cracks resulting from stress corrosion which are mainly intercrystalline.

#### **§4.5. Conclusions:**

The following conclusions can be derived from the experimental findings and discussions.

- (1) Weld microstructure showed predominantly acicular ferrite with dislocation substructure which is a desired microstructure. However, the tempered microstructure in the GRHAZ/ICHAZ may affect the mechanical properties of the welds.
- (2) The high density of  $\epsilon$ -Cu precipitates of average size of 40 nm were observed which is much higher than the 20 nm size often observed in this class of steel. The larger size of  $\epsilon$ -Cu precipitates may be due to overaging effect.
- (3) Spherical aluminosilicate inclusions containing titanium have been observed in the weld-3. This may influence the mechanical properties of the weld.

(4) Cracks revealed by SEM infers the crack propagation direction. The features and service conditions are indicative of corrosion fatigue cracks. The corrosion fatigue cracking results from combination of, i) vibration, ii) susceptible microstructure, and iii) corrosive environment.

### REFERENCES

- (1) G. T. Hahn, *Met. Trans.* **15A** (1984) 947.
- (2) R. E. Dolby, *Welding J.* **58** (1979) 225s.
- (3) O. M. Akselsen and J. K. Solberg, *Mat. Sci. & Tech.* **3** (1987) 649.
- (4) M. Kowaka and S. Nagata, *Corrosion* **32** (1976) 395.
- (5) E. Kunze, G. Gerken and J. Nowak, *Werk. Korr.* **30** (1979) 641.
- (6) W. E. Berry and J. H. Payer, *American Gas Association Journal* (1979) 251.
- (7) P.A. Lefrancois and W. B. Hoyt, *Corrosion* **19** (1963) 360.
- (8) H. J. Grabke, R. Krajak and J. C. Novapaz, *Corrosion Sci.* **35** (1993) 1141.
- (9) A. D. Wilson, E. G. Hamburg, D. J. Colvin, S. W. Thompson and G. Krauss, *Proc. Microalloying 88*, World Materials Congress, ASM International, Metals Park, OH, 1988, pp 269-75.
- (10) M. Mujahid, A. K. Lis, C. I. Garcia and A. J. DeArdo, *Processing, Microstructure and Properties of HSLA Steels*, Eds. A. J. DeArdo, TMS, Warrendale, PA, 1988, pp 345-56.
- (11) G. R. Speich and T. M. Scoonover, *Processing, Microstructure and Properties of HSLA Steels*, Eds. A. J. DeArdo, TMS, Warrendale, PA, 1988, pp 263-85.
- (12) R. Varughese and P. R. Howell, *Mater. Characterisation*, **30** (1993) 261-67.
- (13) S. W. Thompson, D. J. Colvin and G. Krauss, *Met. Trans.* **21A** (1990) 1493-1507.
- (14) R. D. Port, *CORROSION/84*, paper No. 225, NACE, Houston, Texas, 1984.

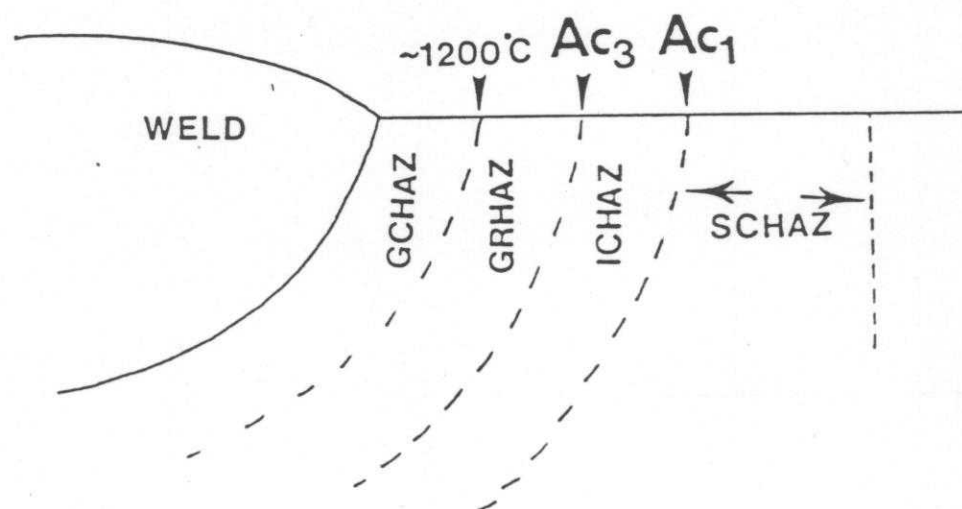


Fig. 1: Schematics of microstructural regions within HAZ.

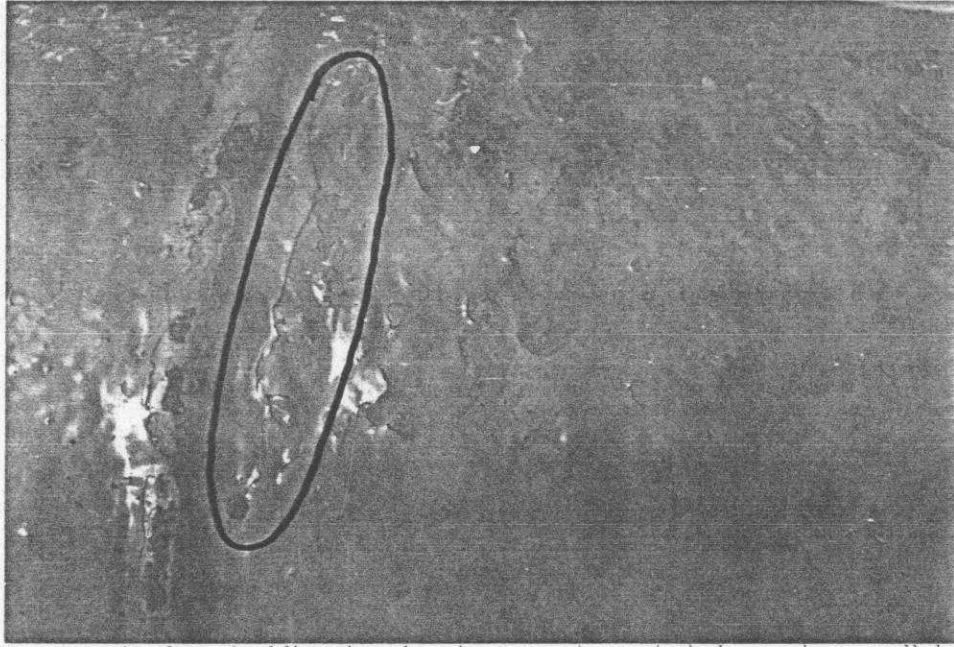
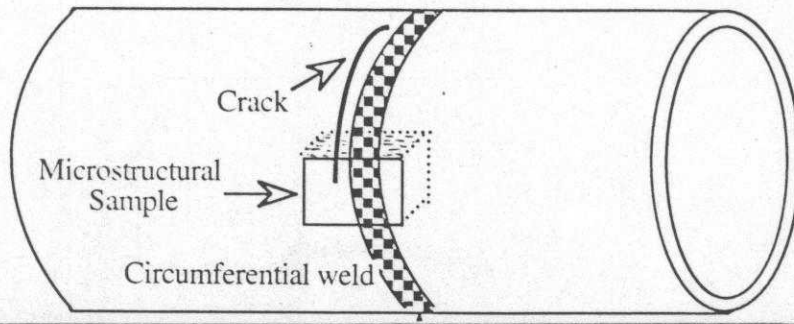


Fig. 2: Photograph of cracked linepipe showing a crack (encircled) running parallel to the circumferential weld.

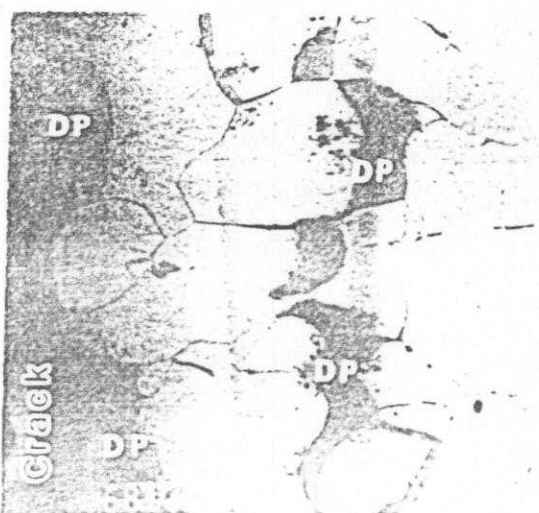


Fig. 3: SEM micrograph from cracked linepipe showing back-scattered electron image of 'dark phase' (marked DP).

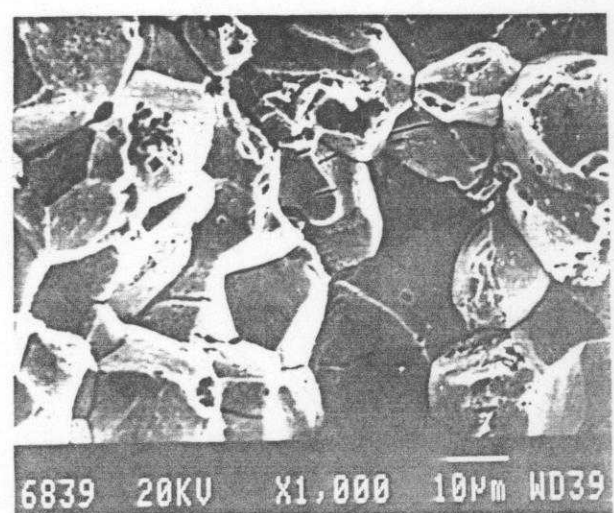


Fig. 4: SEM fractograph of service cracked linepipe A. showing intergranular (IG) brittle fracture.

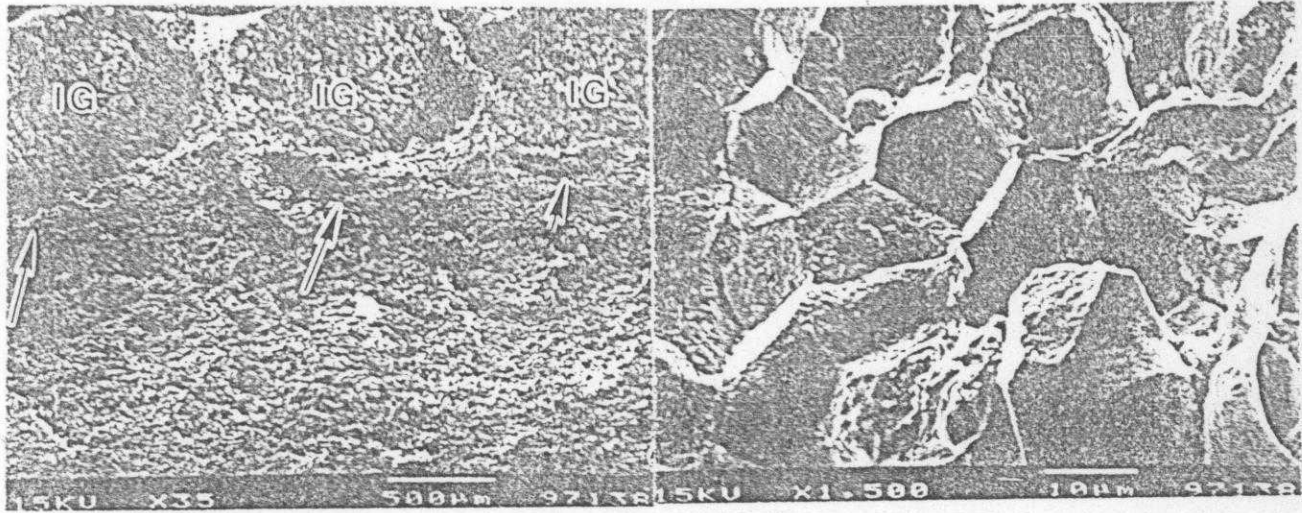


Fig. 5(a): SEM fractograph of tensile test sample C-1 showing three elliptical patches marked by arrows.

Fig. 5(b): higher magnification of patchy regions revealing IG brittle fracture while rest of the surface showed dimple rupture

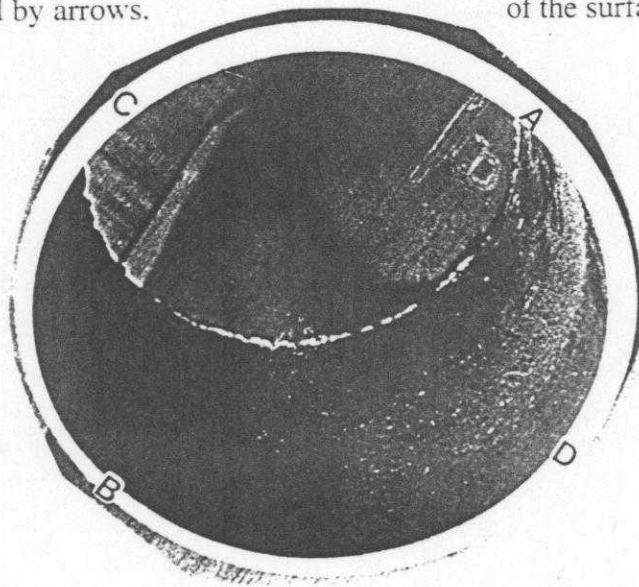


Fig. 6: Photograph of transverse section of tube showing maximum and minimum wall thickness regions marked "A" and "B" respectively. Non-uniform wall thinning can be noticed.

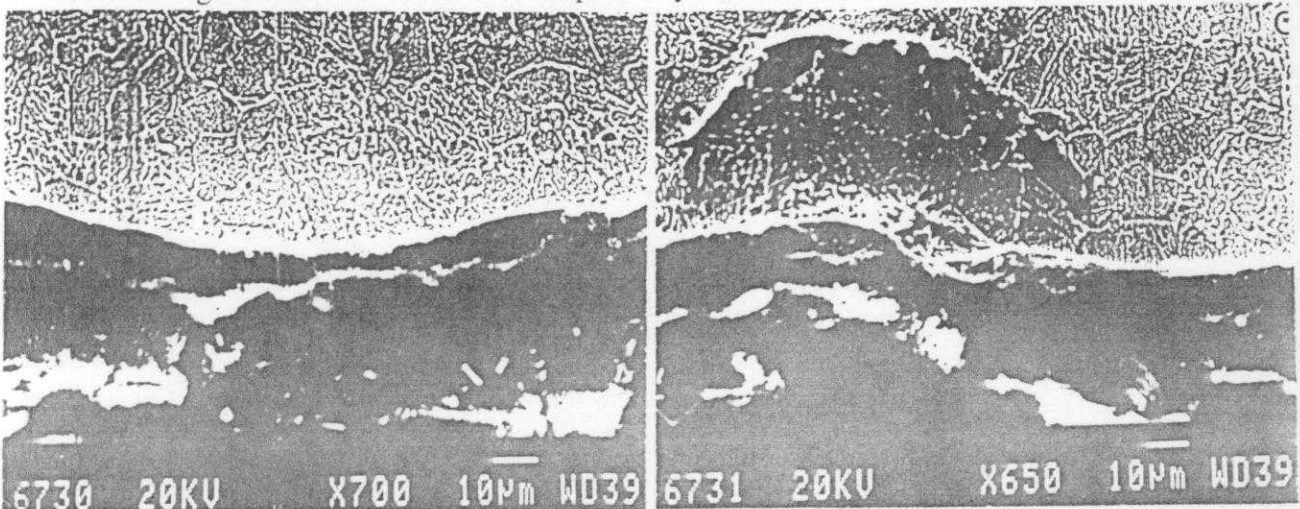


Fig. 7(a): SEM micrograph of transverse section of tube region "A" showing inner tube surface-matrix interface.

Fig. 7(b): SEM micrograph showing pitting initiation at the inner tube surface.

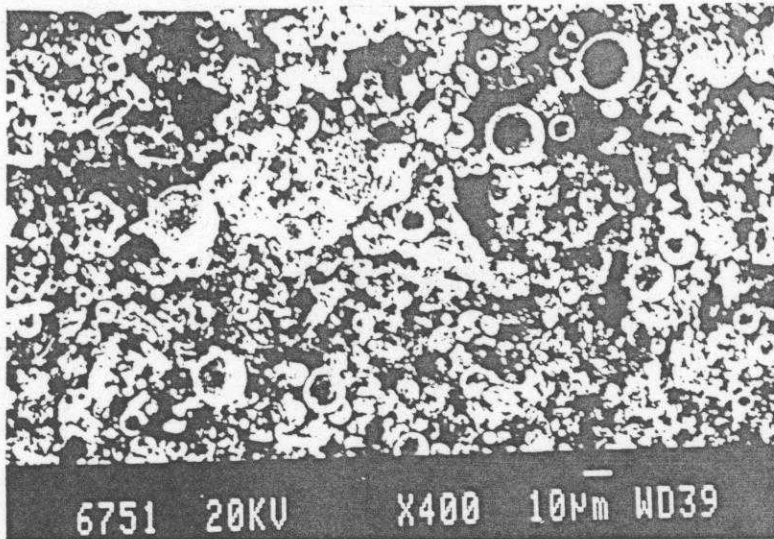


Fig. 8: SEM micrograph of as-received inner tube surface of region "B" showing distribution of spherical metal particles.

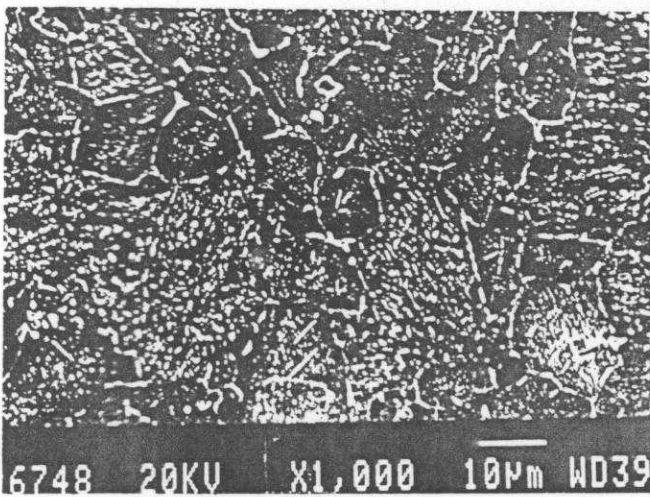


Fig. 9(a): SEM micrographs of transverse section of tube region "B" showing matrix microstructure.

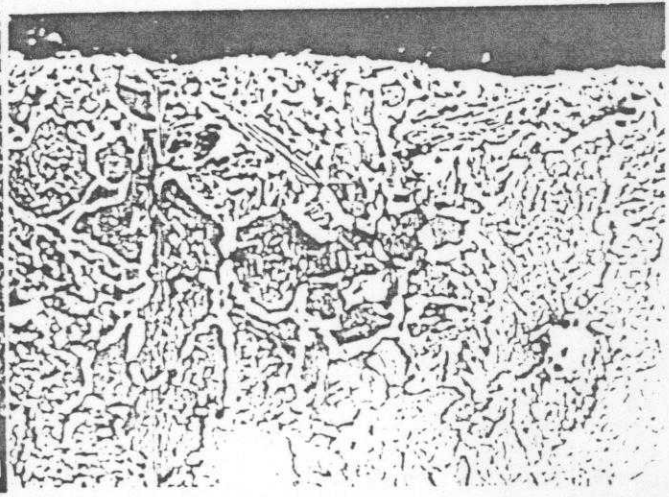


Fig. 9(b): SEM micrograph showing altered microstructure in subsurface region of inner tube wall.

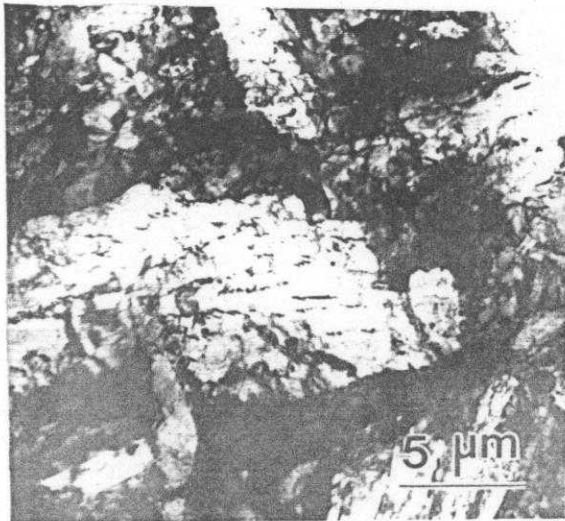


Fig. 10: TEM micrograph of parent metal.

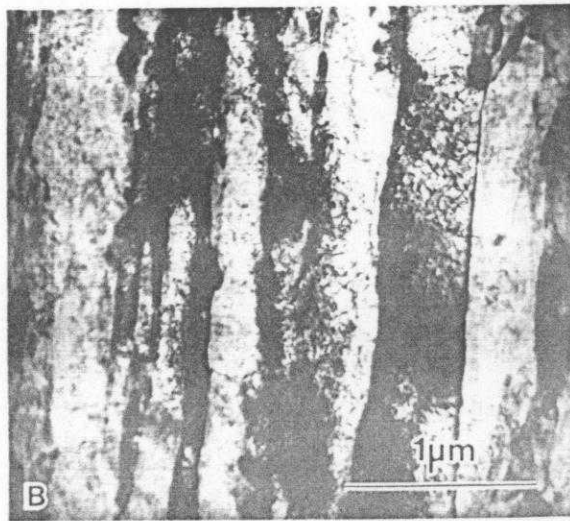


Fig. 11: TEM micrograph of vortex breaker weld-1 showing mainly acicular ferrite with dislocation substructure.

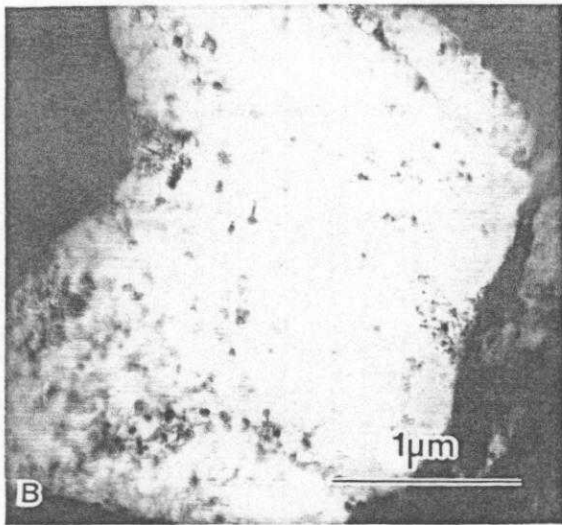


Fig. 12: TEM micrograph showing  $\epsilon$ -Cu precipitates in a blocky ferrite grain.

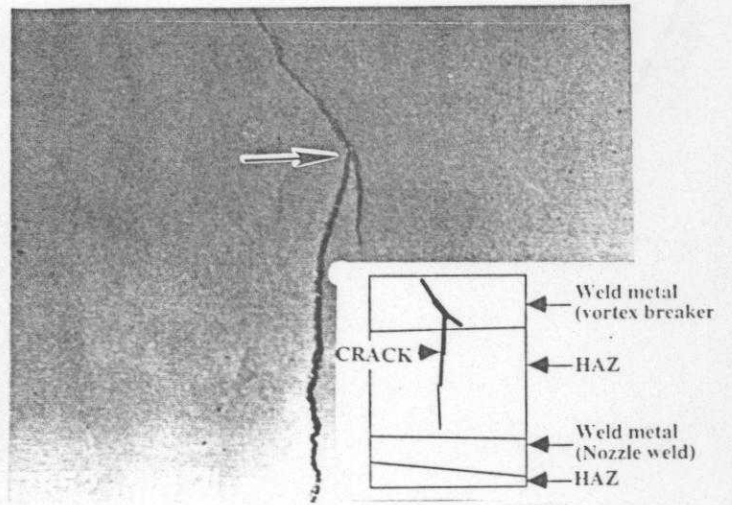


Fig. 13: A low magnification SEM micrograph showing cracks along with its schematic drawing.

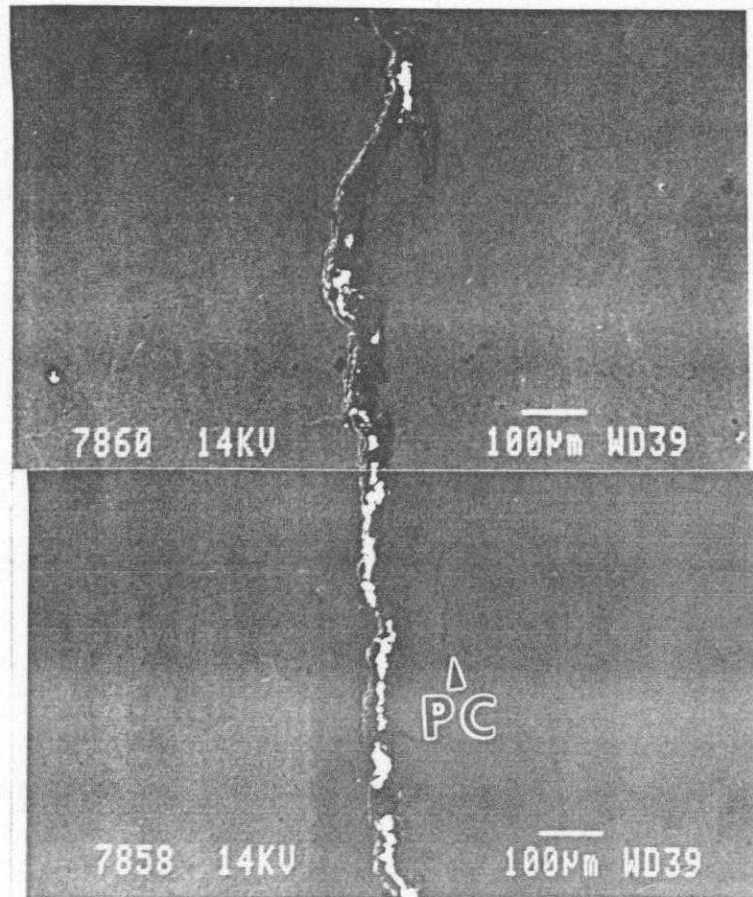


Fig. 14: A higher magnification montage of SEM micrographs showing main crack and localized parallel crack, marked "PC".